Rapid Synthesis of Nanostructured Pure Anatase TiO_2 with High Thermal Stability by Polymeric Sol-Gel Route

V. Tajer-Kajinebaf[1], H. Sarpoolaky [1]

Abstract

The nanostructured anatase TiO_2 with high thermal stability was prepared by polymeric sol-gel method without any additives. The particle size distribution of polymeric titania sol was determined by dynamic light scattering (DLS). The properties of prepared titania were investigated by TG-DTA, XRD, FESEM and TEM. The decolorization capability of resultant anatase was also evaluated using methyl orange photodegradation in aqueous solution by UV–visible spectrophotometer. The results of DLS showed the particle size distribution of the polymeric sol is in the range of 0.5-2 and 1-3 nm after 1 and 50 days, respectively. Titania prepared by polymeric method showed high thermal stability against phase transformation from anatase to rutile. Also, crystallite size of anatase calcined at 400-750 °C was in the range of 10-50 nm. The prepared nanostructured anatase showed an acceptable decolorization capability for methyl orange degradation.

Keywords: Nanostructure; Anatase; Sol-Gel; Thermal Stability; Decolorization

1. Introduction

Titania is a reference material in the term of photocatalytic efficiency under UV-irradiation, with well-established technological applications [1]. The use of titanium dioxide as a photocatalyst in the destruction of organic pollutants [2, 3] and dyes [4-8] has been recently become interesting research topic. However, TiO2 has the ability to degrade organic materials and dyes on surface of titania via photocatalysis in the presence of UV-light and an oxygen source [9]. Nowadays, there are many proposed innovative and commercial ceramic applications for titania-coated materials such as bathroom tiles, sanitary wares, and self-cleaning glass for the control of organic contaminants and decolorization that require high processing temperatures and hence high thermal stability [10]. Among the different forms of titania, anatase is the most photoactive form [11-13] but it is thermodynamically metastable. Also, the relatively low surface area and anatase-rutile transformation at high temperatures are disadvantages. The phase transformation requires movement of cations and anions which leads to mass transport during conversion and rapid loss of surface area upon sintering [14]. The transformation temperature of anatase to rutile depends on the initial (anatase) particle size, synthesis route, dopants and impurities. Therefore, it is of interest to develop methods that increase the anatase-rutile transformation temperature. The studies show the anatase phase is generally converted to the rutile at temperatures lower than 600 °C [15-17]. Many researchers have tried to increase the thermal stabilization of titania [11, 18, 19]. The most popular methods are the use of dopants and additives like zirconia [14, 20, 21], alumina [22-25] and silica [26-29]. Although, the as-prepared samples are mostly amorphous and additives form impurity phases at higher temperatures. Recently, it has been observed that the different synthesis routes such as sol-gel, hydrothermal [29-31], microwave-assisted hydrothermal [18, 32, 33], chemical vapor synthesis (CVS) [34] and ultrasonic spray pyrolysis [35, 36] has also great effect on the transformation temperature. Although successful results are given using these methods but sol-gel route is still increasingly of interest due to easy and fast. To our knowledge, the use of TTIP as

1- School of Metallurgy and Materials Engineering, Iran University of Science & Technology, 16846-13114, Tehran, Iran.

Corresponding author: H. Sarpoolaki, School of Metallurgy and Materials Engineering, Iran University of Science & Technology, 16846-13114, Tehran, Iran.
Email: hsarpoolaky@iust.ac.ir

direct starting material via polymeric sol-gel route has not been reported for preparation of nanostructured anatase with high temperature stability. In the present work, polymeric sol-gel route as a very easy, fast and reproducible method is introduced to produce anatase nanopowders with the high thermal stability without any additives. The synthesis conditions are discussed first, and then molar ratio and subsequently heat-treatment conditions are introduced to produce anatase nanopowder. The thermal and structural evolutions of the resultant titania are then studied and finally, the results on the decolorization properties of nanostructured anatase are presented.

2. Experimental

Titanium tetraisopropoxide (TTIP, Ti $(OC_3H_7)_4$, Merck 821895), isopropanol (IPA, C3H7OH, Merck 109634), hydrochloric acid (HCl 37% solution, Merck 100317) and deionized water were used as raw materials. Titania polymeric sol was obtained by hydrolysis of TTIP via the addition of a less than equivalent amount of H_2O ($[H_2O]/[Ti] < 4$) in order to obtain a precipitate free polymeric sol. A solution of water and hydrochloric acid as a catalyst in isopropanol was added dropwise to a solution of TTIP and isopropanol during high speed stirring. The molar ratio for TTIP: IPA: H2O: HCl of the final sol was 1:31:0.8:0.23, respectively.

Stirring was continued for 4 h to get a stabilized sol. The final product was a transparent polymeric titania sol. For gel preparation, a part of the polymeric sol was dried at room temperature for 24 h. Then, the resultant dried gel was subsequently calcined at temperatures of 400, 550, 650, 750 and 850 °C in air for 1 h with a heating rate of 1 °C/min. The particle size distribution of polymeric sol was determined by the dynamic light scattering technique (DLS Malvern, UK, and ZS3600).

Thermal properties of the dried gel were characterized by thermogravimetric analysis (DTA-TG PERKINELMER) in a nitrogen flow with a heating rate of 7.5 °C/min in the temperature interval 25-900 °C. The phase composition and the average crystallite size of the gel calcined at different temperatures were identified using X-ray diffraction technique with CuKα wavelength at 30 mA and 40 kV (XRD, Jeol JDX-8030). Microstructure of titania was characterized using field emission scanning electron microscopy (FESEM MIRA\\TESCAN) and transmission electron microscopy (TEM, EM 208, Philips) with an accelerating voltage of 30 and 100 kV, respectively. The decolorization capability of the prepared anatase nanopowder was measured by the degradation of methyl orange in an aqueous solution. 3 mg catalyst per mL solution (20 mg/lit) was irradiated by a UV source (Sunny, 360–415 nm, 125 W). After 70 min UV-radiation, the concentration of methyl orange solution was examined by UV-visible spectrophotometer (Agilent, 8453).

3. Result and Discussion

3.1. Particle Size Distribution

Fig. 1 shows the particle size distribution of the polymeric sol after 1 and 50 days that is in the range of 0.5-2 and 1-3 nm, respectively.

Fig. 1(a,b) shows that particle size of the polymeric titania sol increases after 50 days. Previous works showed that by adding a small amount of water, the hydrolysis reaction is done slowly, resulting in a partially hydrolyzed alkoxide and the formation of a linear inorganic polymer [37]. This is obvious in Fig. 1 (c). It seems at the beginning of condensation reaction, the size of branched polymers is very small. However, during aging, the number and length of branched polymers increase due to the development of condensation reaction which is clearly seen in Fig. 1 (d).

3.2. Thermal Analysis

To determine the transformation temperature of TiO_2, the dried gel was subjected to thermogravimetric analysis. The results are shown in Fig. 2.

The pattern follows 45% weight loss during three steps. The first weight loss (22%) which is up to 200 °C is accompanied by an endothermic peak in the DTA curve. This

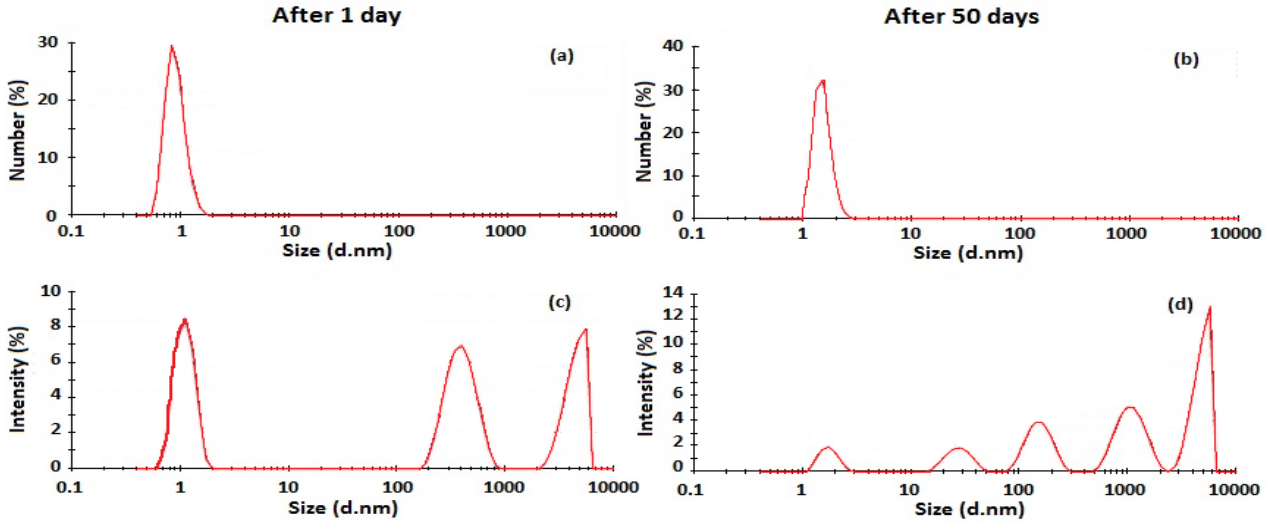

Fig. 1. The particle size distribution of titania polymeric sol:
a,b) plots of number (%) versus size (nm) after 1 and 50 days, respectively;
c,d) plots of intensity (%) versus size (nm) after 1 and 50 days, respectively.

peak is attributed to the removal of adsorbed water, alcohol and bound water [38].

The second and third weight losses (5 and 18%, respectively) are accompanied by a series of exothermic reactions which is attributed to the combustion of organic compounds and the decomposition of the hydroxyl group ($Ti(OH)_4$).

The broad exothermic peak corresponding to third step can be attributed to TiO_2 phase transition of amorphous to anatase. There is no peak corresponding to anatase-rutile phase transition up to 900 °C. During the decomposition of $Ti(OC_3H_7)_4$ in the presence of oxygen, each mole of TTIP reacts with 18 moles of oxygen to produce one mole of TiO_2, 12 moles of CO_2 and 14 moles of H_2O according to the following chemical reaction [39]:

$$Ti(OC_3H_7)_4 + 18O_2 \rightarrow TiO_2 + 12CO_2 + 14H_2O \quad (1)$$

while, in the absence of oxygen, $Ti(OC_3H_7)_4$ is decomposed according to the following reaction:

$$Ti(OC_3H_7)_4 \rightarrow TiO_2 + 4C_3H_6 + 2H_2O \quad (2)$$

when titania is synthesized at a lower O_2/He flow rate ratio, a greater proportion of TTIP decomposed according to reaction 2 and some of the resulting hydrocarbon is deposited as a powder. By heating this powder under oxygen atmosphere all the carbon got oxidized. On the other hand, when the O_2/He flow rate ratio is high, a larger quantity of CO_2 is generated according to reaction 1. According to the previous research, this is probably because of the presence of carbon in the titania structure which postpones the phase transformation from anatase to rutile [34]. So, the anatase-rutile transformation may be suppressed due to remain carbon in titania structure that prevents atoms arrangement.

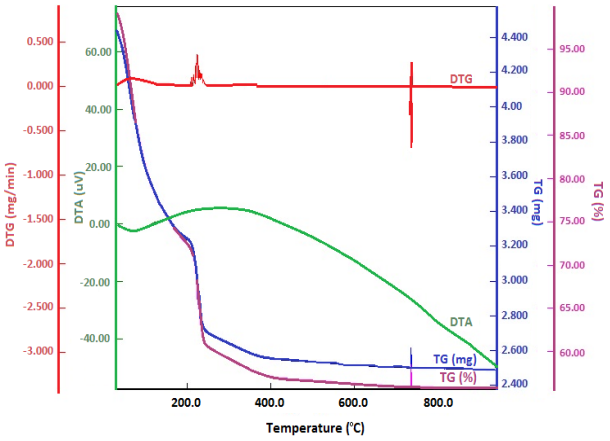

Fig. 2. The thermogravimetric curve of the dried polymeric titania gel.

3.3. Structural Properties

The XRD patterns of the titania gel calcined at different temperatures are shown in Fig. 3.

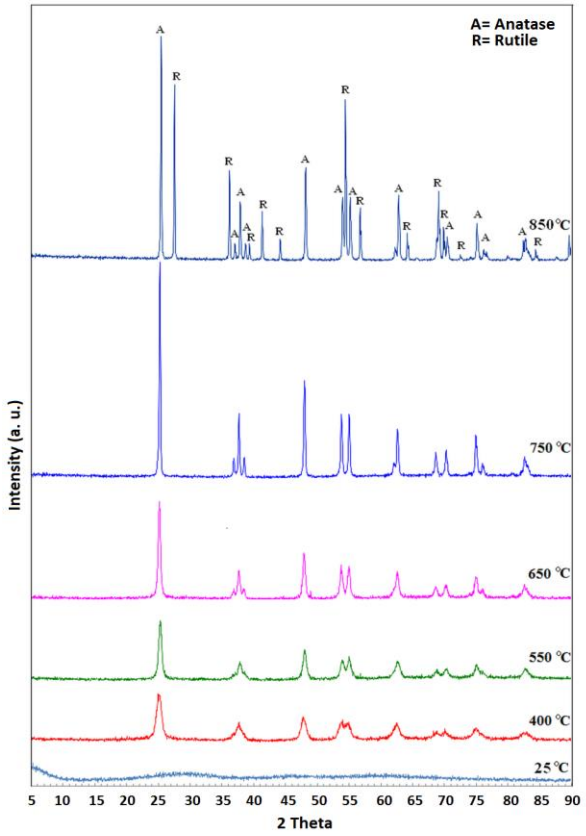

Fig. 3. XRD patterns of the gel calcined at different temperatures.

The XRD pattern of the dried gel shows fully amorphous phase. It is well shown that anatase peaks appear during calcination process.

These peaks become sharper with increasing calcination temperature up to 750 °C. The characteristic rutile peaks appear at 850 °C. However, the crystallization temperature recorded by the thermo gravimetric analysis is slightly higher than that obtained by XRD. This can be attributed to the fact that heating rate in DTA/TG apparatus (7.5 °C/min) is more than that of the heat-treatment furnace (1 °C/min).

The average crystallite size is calculated from the line broadening of X-ray diffraction peak using the Scherrer's equation as expressed by Eq. (1) [29]:

$$L=K\lambda/\beta \cos\theta \quad (1)$$

where L is the crystallite size, k is the Scherrer constant usually taken as 0.89, λ is the wavelength of the X-ray radiation (0.15418 nm for CuKα), and β is full width half maximum (FWHM) of diffraction peak measured at 2θ. The FWHM value was extracted from the XRD pattern fitted using the X'Pert HighScore software. Also, the anatase weight ratio (WA) was estimated from XRD intensity data by using Eq. (2):

$$WA = 1 - [1 + 0.8IA/IR]-1 \quad (2)$$

where I_A and I_R represent X-ray integrated intensity of (101) reflection of anatase and (110) reflection of rutile, respectively [29]. Also, the lattice strain percentage was determined by new X'pert software. The results are recorded in the Table 1.

The results show that titania prepared by polymeric sol-gel route has higher thermal stability against anatase-rutile phase transformation. No significant rutile peak is observed for the gels calcined up to 750 °C according to the absence of the (110) rutile reflection at 2θ = 27.4°. It seems that the transformation is suppressed due to the presence of carbon at high temperatures as previously described. Since the anatase is the most photoactive polymorph of titania [11-13], this result would be attractive for photocatalytic applications.

Table 1. Decrease of the maximum residual stress in fiber and matrix.

Temp. (°C)	Phase		Crystallite Size (nm)		W_A	Lattice Strain (%)
	Major	Minor	Major	Minor		
25	Amorph	-	-	-	1	-
400	Anatase	-	9.6	-	1	1.689
550	Anatase	-	21.8	-	1	0.763
650	Anatase	-	27.6	-	1	0.614
750	Anatase	-	46.0	-	1	0.382
850	Anatase	Rutile	59.4	59.7	0.51	0.301

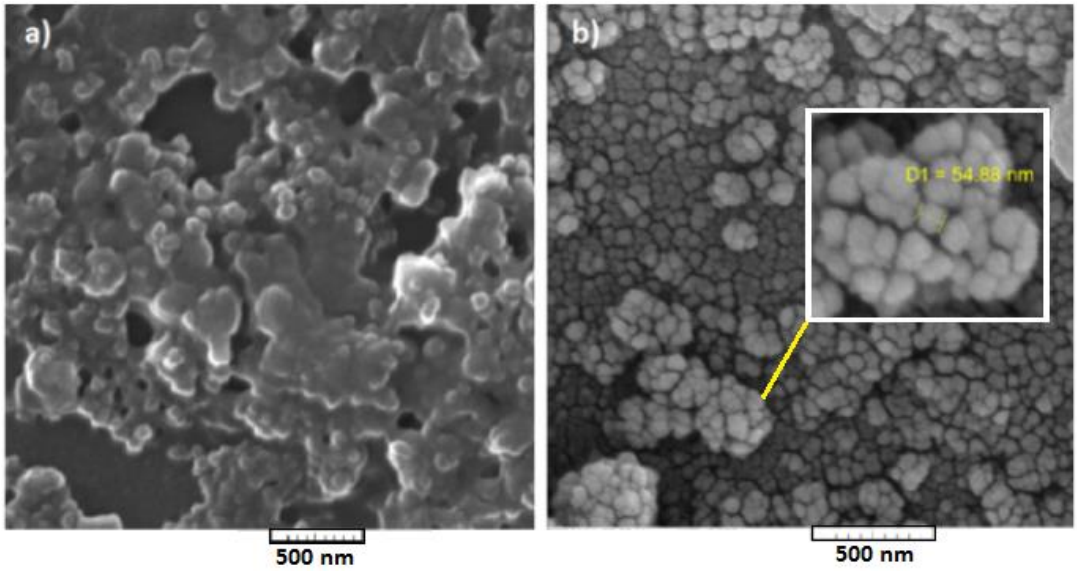

Fig. 4. FESEM images of the resultant samples: a) dried titania gel and b) heat treated titania powder.

3.4. Morphology

FESEM images of the nanostructured anatase powder are shown in Fig. 4.

SEM image of the dried polymeric sol (gel) shows that agglomerates consist of nanometer spherical particulates (Fig. 4a). Figs. 4(b,c) also show the particles of the gel calcined at 400 °C are smaller than 50 nm (Fig. 4c) that is in accordance with the average crystallite size calculated by the Scherrer's equation (Table 1). Therefore, according to these images, anatase nanopowder can be produced by polymeric sol-gel route.

Also, TEM image (Fig. 5) shows that anatase powder calcined at 400 °C is composed of particle in nanometer scale (10–20 nm). These results are in agreement with XRD results.

3.5. Decolorization Capability

Fig. 6 compares the concentration changes of methyl orange aqueous solution in the presence of prepared anatase nanopowder under UV-radiation in different times.

The removal efficiency of dye can be estimated by applying the following Eq. (3):

$$\text{Removal efficiency (\%)} = [(C_0\text{-}C)/C] \times 100 \qquad (3)$$

Where C_0 is the original methyl orange content and C is the residual methyl orange in solution [40]. These results show that the amount of absorbed methyl orange solution in 480 nm wavelength after 0, 30 and 70 min is 1.428, 0.551 and 0.026, respectively. Thus, the removal efficiency (%) after 30 and 70 min is obtained 61% and 98%, respectively. So, the decolorization capability of the prepared anatase nanopowder would be acceptable.

Fig. 7 shows the concentration changes of methyl orange solution in the presence of anatase nanopowder calcined at different temperatures after 70 min UV-radiation. According to Fig. 7, titania calcined at 400 °C shows the highest decolorization capability.

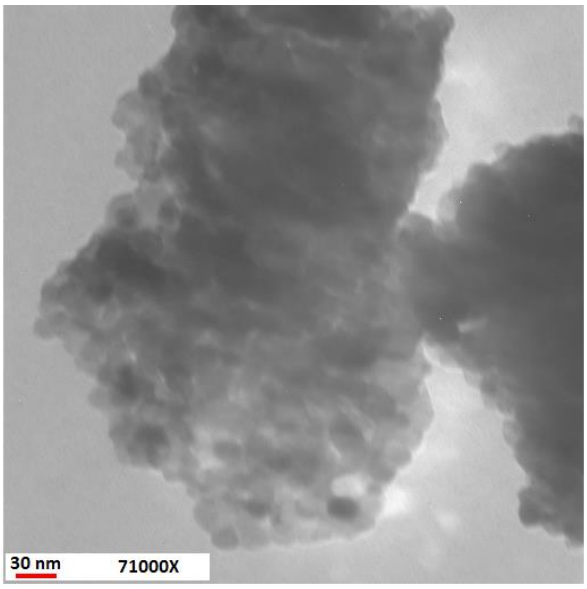

Fig. 5. TEM micrograph of the nanostructured anatase particles.

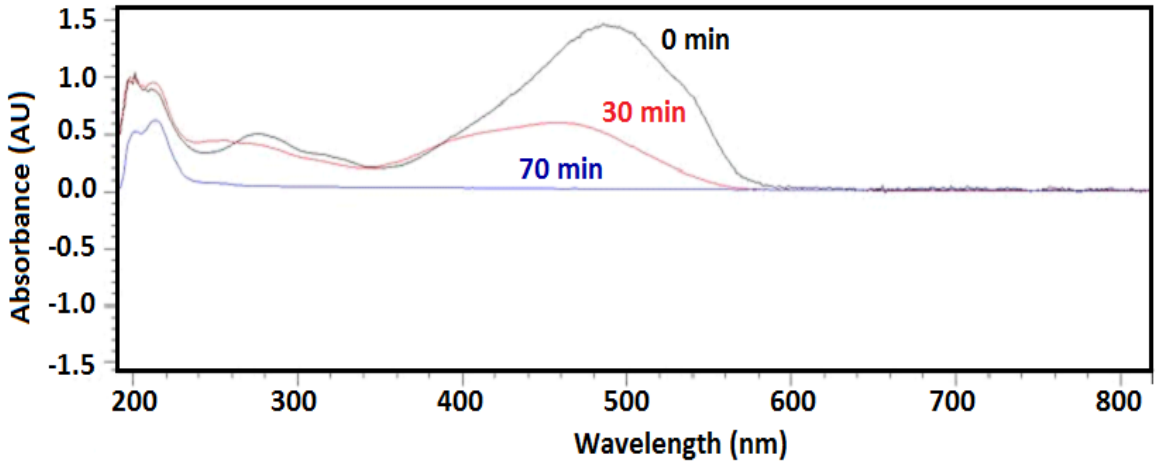

Fig. 6. Concentration changes of methyl orange aqueous solution in different times under UV-radiation.

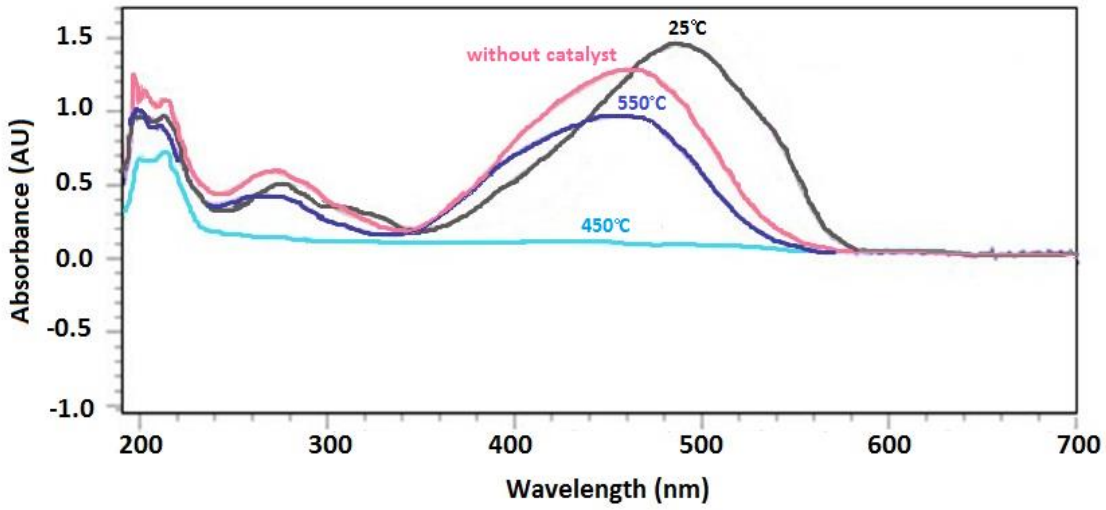

Fig. 7. Concentration changes of methyl orange solution for anatase nanopowder calcined at different temperatures.

These results indicate that despite the increase of the anatase peak intensity by increasing calcination temperature, the decolorization capability decreases. This may be related to larger crystallite size of titania calcined at higher temperatures that reduces the surface area of anatase powder (according to Table 1).

4. Conclusions

In the present work, the nanostructured pure anatase nanopowder with high thermal stability was synthesized via a simple polymeric sol-gel route. The particle size distribution of the polymeric titania sol was in the range of 0.5-2 and 1-3 nm after 1 and 50 days, respectively. Titania prepared by polymeric sol-gel route showed higher thermal stability against anatase-rutile phase transformation. Also, crystallite size of anatase calcined at 400-750 °C was in the range of 10-50 nm. The prepared anatase also showed an acceptable decolorization capability for methyl orange degradation in an aqueous solution. The dye removal efficiency of the nanostructured anatase was obtained 98% after 70 min of radiation.

References

1. A. Fujishima, K. Hashimoto and T. Watanabe, TiO_2 Photocatalysis, *Fundamentals and Applications*, (BKC Inc., Tokyo), 2001.
2. A. Kafizas, S. Kellici, J.A. Darr and I.P. Parkin: *J. Photochem. Photobiol., A* 2044 (2009) 183-190.

3. H. Zhang, X. Quan, Sh. Chen, H. Zhao and Y. Zhao: *Sep. Purif. Technol.*, 50 (2006) 147-155.
4. A. Hosseinnia, M. Keyanpour-Rad and M. Pazouki: *World Appl. Sci. J*., 8(11) (2010) 1327-1332.
5. A.K. Subramani, K. Byrappa, S. Ananda, K.M. Lokanatha Rai, C. Ranganathaiah and M. Yoshimura: *Bull. Mater. Sci*., 30(1) (2007) 37-41.
6. Ch.Ch. Liu, Y.H. Hsieh, P.F. Lai, Ch.H. Li and Ch.L. Kao: Dyes Pigm., 68 (2006) 191-195.
7. N.M. Mahmoodi and M. Arami: *Chem. Eng. J*., 146 (2009) 189-193.
8. S. Mozia, A.W. Morawski, M. Toyoda and M. Inagaki: Desalination, 241 (2009) 97-105.
9. A. Kafizas, S. Kellici, J.A. Darr and I.P. Parkin: *J. Photochem. Photobiol*., A, 204 (2009) 183-190.
10. U. Stafford, K.A. Gray, P.V. Kamat and A. Varma: *Chem. Phys. Lett.*, 205(1) (1993) 55-61.
11. A.L. Castro, M.R. Nunes, A.P. Carvalho, F.M. Cost, and M.H. Florecˆncio: *Solid State Sci*., 10 (2008) 602-606.
12. L. Djafera, A. Ayral and A. Ouagued: Sep. Purif. Technol., 75 (2010) 198-203.
13. Ch. He, B. Tian and J. Zhang: *J. Colloid Interface Sci.*, 344 (2010) 382-389.
14. D.J. Reidy, J.D. Holme and M.A. Morris: *Ceram. Int*., 32 (2006) 235-239.
15. Ch.H. Kwon, J. H. Kim, I.S. Jung, H. Shin and K.H. Yoon: *Ceram. Int*., 29 (2003) 851-856.
16. T. Kawahara, T. Ozawa, M. Iwasaki, H. Tada and S. Ito: *J. Colloid Interface Sci*., 267 (2003) 377-381.
17. J. Kim, K.Ch. Song, S. Foncillas and S.E. Pratsinis: *J. Eur. Ceram. Soc*., 21 (2001) 2863-2872.
18. K. Lv, J. Yu, L. Cui, Sh. Chen and M. Li: J. Alloys Compd., 509 (2011) 4557-4562
19. D. He and F. Lin: *Mater. Lett.*, 61 (2007) 3385-3387.
20. J. Sekuli, A. Magraso, J.E. ten Elshof and D.H.A. Blank: Microporous Mesoporous Mater., 72 (2004) 49-57.
21. K.Y. Jung and S.B. Park: *Mater. Lett.*, 58 (2004) 2897-2900.
22. Y.S. Jung, D.W. Kim, Y.S. Kim, E.K. Park and S.H. Baeck: *J. Phys. Chem. Solids*, 69(5-6) (2008) 1464-1467.
23. A.A. Habibpanah, S. Pourhashem and H. Sarpoolaky: *J. Eur. Ceram.* Soc., 31 (2011) 2867-2875.
24. K.N.P. Kumar: *Appl. Catal.*, A, 119(1) (1994) 163-183.
25. K.N.P. Kumar: *Scr. Metall. Mater*., 32(6) (1995) 873-877.
26. K.G.K. Warrier, S.R. Kumar and C.P. Sibu: *J. Porous Mater*., 8 (2001) 311-37.
27. A. Ennaoui, B.R. Sankapal, V. Skryshevsky and M.Ch. Lux-Steiner: *Sol. Energy Mater. Sol. Cells*, 90 (2006) 1533-1541.
28. J. Yu AND J.C. Yu: *J. Sol-Gel Sci. Technol*., 24 (2002) 95-103.
29. Zh. Li, B.Hou, Yao Xu, D. Wu, Y. Suna, W. Hu and F. Deng: *J. Solid State Chem*., 178 (2005) 1395-1405.
30. M. Toyoda, Y. Nanbu, Y. Nakazawa, M. Hirano and M. Inagaki: *Appl. Catal*., B, 49 (2004) 227-232.
31. T. An, J. Liu, G. Li, Sh. Zhang, H. Zhao, X. Zeng, G. Sheng and J. Fu: *Appl. Catal., A*, 350 (2008) 237-243.
32. L. Cui, K.N. Hui, K.S. Hui, S.K. Lee, W. Zhou, Z.P. Wan and Chi-Nhan Ha Thuc: *Mater. Lett*., 75(15) (2012) 175-178.
33. Y. Zheng, K. Lv, Zh. Wang, K. Deng and M. Li: J. Mol. Catal. *A: Chem*., 356 (2012) 137-143.
34. M. I. Ahmad, C. Fasel, T. Mayer, S.S. Bhattacharya and H. Hahn: *Appl. Surf. Sci*., 257 (2011) 6761-6767.
35. A. Nakaruk, D. Ragazzon and C.C. Sorrell: Thin Solid Films, 518 (2010) 3735-3742
36. N.C. Raut, T. Mathews, P. Chandramohan, M.P. Srinivasan, S. Dash and A.K. Tyagi: *Mater. Res. Bull*., 46(11) (2011) 2057-2063.
37. T. Tsuru: *J. Sol-Gel Sci. Technol*., 46 (2008), 349-361.
38. A.J. Patil, M.H. Shinde, H.S. Potdar, S.B. Deshpande, S.R. Sainkar, S. Mayadevi and S.K. Date: Mater. *Chem. Phys*., 68 (2001) 7-16.
39. S.Y. Kim, J.H. Yu and J.S. Lee*: Nanostruc. Mater*., 12(1-4) (1999) 471-474.
40. A.A. Ismail, I.A. Ibrahim, M.S. Ahmed, R.M. Mohamed and H. El-Shall: *J. Photochem. Photobiol.*, A, 163 (2004) 445-451.